ADVANCED FUNCTIONAL MATERIALS
www.afm-journal.de

Long Range Self-Assembly of Polythiophene Breath Figures: Optical and Morphological Characterization

Prahlad K. Routh, Dmytro Nykypanchuk, T. A. Venkatesh, and Mircea Cotlet**

Large-area, device relevant sized microporous thin films are formed with commercially available polythiophenes by the breath figure technique, a water-assisted micropatterning method, with such semitransparent thin films exhibiting periodicity and uniformity dictated by the length of the polymer side chain. Compared to drop-casted thin films, the microporous thin films exhibit increased crystallinity due to stronger packing of the polymer inside the honeycomb frame.

1. Introduction

Ordered microporous polymer films have gained increased attention in the past several years as they are being explored for potential applications in soft lithography,[1] tissue engineering,[2] catalysis,[3] and as superhydrophobic surfaces.[4] The regularity of pore size and the long-range order is the most sought out feature for many of these applications and this has been a long standing challenge with the breath figure technique (BFT).[5] There are a variety of bottom-up and top-down patterning techniques such as photolithography, electron beam lithography, chemical etching, and printing techniques for producing ordered microstructures.[6] Although the versatility of structures produced by lithographic techniques is large, the initial cost of equipment and the needed skilled labor are high. Hence, there has been a stress recently on low-cost techniques to produce highly ordered structures with tunable pore size using self-assembly.[7] BFT is one such method, which is driven by water-based self-assembly. In BFT, a polymer is dissolved in a low boiling point solvent and casted on a substrate in high humidity atmosphere. Spontaneous evaporation of the volatile solvent leads to a decrease in temperature of the top surface of the solution (–6 to 0 °C).[8] As a result of this temperature drop, small water droplets condense on the surface of the solution. These microdroplets grow with time ($D \approx t^{1/3}$, D, diameter, t, time) but when they come in contact with another droplet, they do not tend to coalesce.[9] The polymer precipitates between these water microspheres, preventing them from coalescing with each other. As a result, these uniform sized microspheres of water droplets arrange themselves in a hexagonally packed pattern on the top of solution. After solvent evaporation and subsequent evaporation of water, a thin polymer film is left with the imprint of cavities created by the hexagonally arranged microspheres. Such pattern is usually referred to as a honeycomb pattern. The long-range order and regularity of honeycomb patterns depend on various experimental parameters such as humidity, molecular weight of polymer, solvent, polymer concentration, temperature, and the nature of the substrate used for deposition.[10] These parameters control the evaporation rate of the solvent, prevent coalescing of water droplets, and affect the honeycomb final film morphology. The effects of these experimental parameters were summarized in several review papers.[8,11] The dynamics of this seemingly simple method is rather complex due to the Marangoni convection currents generated by temperature gradient.[8,12] Hence, the apparatus deposition design and the precise control of these experimental parameters become extremely important for achieving reproducibility of ordered honeycomb patterns. Several mechanisms have been proposed to explain the heterogeneity seen in the BFT process and it is also believed that there could be more than one mechanism at interplay during the breath figure process.

There has been a recurring debate as to which polymer type can form honeycomb patterns by BFT.[11a] Initially it was believed that only polymers with a star shape could form such microstructures,[13] later on honeycomb films were obtained with polystyrene polymers with linear structure and it was proposed that the viscosity of the solution is critical in forming honeycomb patterns.[14] Since then honeycomb patterns have been demonstrated with block copolymers, amphiphilic copolymers, hyperbranched polymers, and organic/inorganic hybrid materials.[15] Recently, BFT has been demonstrated with nonaqueous vapors[16] and on nonplanar substrates.[17] It is believed that some polymer architectures provide a robust set of process parameters which can allow tuning of the honeycomb pore structure, while other polymer architectures provide a narrow range of process conditions which can produce honeycomb morphology, hence making reproducibility difficult.

Honeycomb patterns have also been demonstrated with conductive polymers[18] and such microporous thin films have been recognized for their potential as building blocks for interesting optoelectronic device application areas such as sensing and semitransparent photovoltaics. However, prior studies in the field have relied largely on custom synthesized conjugated polymers for creating relatively small area honeycombs.

P. K. Routh, Dr. D. Nykypanchuk, Dr. M. Cotlet
Center for Functional Nanomaterials
Brookhaven National Laboratory
Upton, NY 11793, USA
E-mail: cotlet@bnl.gov
P. K. Routh, Dr. M. Cotlet, Prof. T. A. Venkatesh
Department of Materials Science and Engineering
Stony Brook University
Stony Brook, NY 11790, USA
E-mail: t.venkatesh@stonybrook.edu

DOI: 10.1002/adfm.201502463

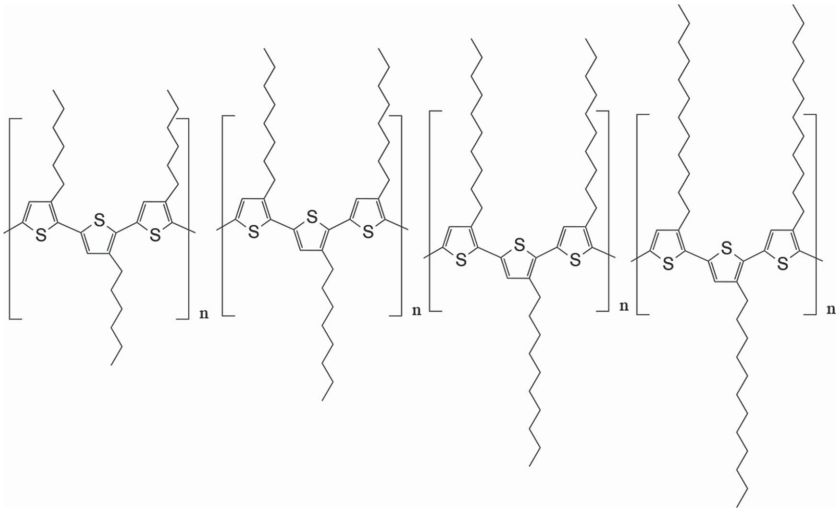

Scheme 1. Polythiophenes with varying side chain length: poly(3-hexyl thiophene), P3HT; poly(3-octyl thiophene), P3OT; poly(3-decyl thiophene), P3DT; and poly(3-dodecyl thiophene), P3DDT.

Furthermore, the relationships between the processing conditions, polymer chemistry, and honeycomb structure formation and their resultant optoelectronic properties have not been fully understood.

Hence, in this present study we focused on developing a BFT method where several important process conditions such as temperature, humidity, and air flow can be controlled and we applied this BFT to a series of commercially available polythiophene (PT) derivatives which differ by the side chain length (**Scheme 1**). These polymers have been previously investigated as organic photovoltaic candidate materials.[19] To compare the honeycomb formation capability of the four PT derivatives versus side chain effect, we have kept processing parameters like regioregularity, concentration, molecular weight, substrate chemistry, and evaporation rate fixed and then studied the effect of increasing side chain length on breath figure forming capability.

We have been able to demonstrate highly ordered microporous thin films with large surface area (≈5 × 5 mm^2), the largest size reported so far for conjugated polymer honeycomb thin films, an achievement making such semitransparent films suitable candidates for sensing and semitransparent photovoltaic applications.

2. Results

2.1. Side Chain Effect on Ordering of Pores

In this study, we used a series of commercial polythiophene conjugated polymers where the alkyl side chain length is varied from $m = 6$ (poly(3-hexyl thiophene) or P3HT), to $m = 8$ (poly(3-octyl thiophene) or P3OT), to $m = 10$ (poly(3-decyl thiophene) or P3DT) and finally to $m = 12$ (poly(3-dodecyl thiophene) or P3DDT) (Scheme 1). These polymers, commercially available from Rieke Metals, were dissolved at similar concentrations in carbon disulfide (CS_2) and were subjected to the same processing conditions in a BFT apparatus described in detail in Figure S1 (Supporting Information) in order to obtain honeycomb films. While BFT films were deposited on various substrates like glass, hydrophilic glass, ITO, MoO_3, and ZnO coated glass, defect free breath figure films were formed mainly on glass coated with oxides, in particular MoO_3, for which all characterization reported herein applies.

Figure 1 shows optical images of the PT-based honeycombs, both at low and high magnification, for all four polymers, demonstrating large area ordered honeycombs. **Figure 2** are scanning electron microscopy (SEM) images of PT-based honeycombs along with fast Fourier transform (FFT) patterns obtained by image processing (see the Supporting Information for details). The hexagonal packing and long-range order can be deduced from such FFT patterns. P3OT shows long-range

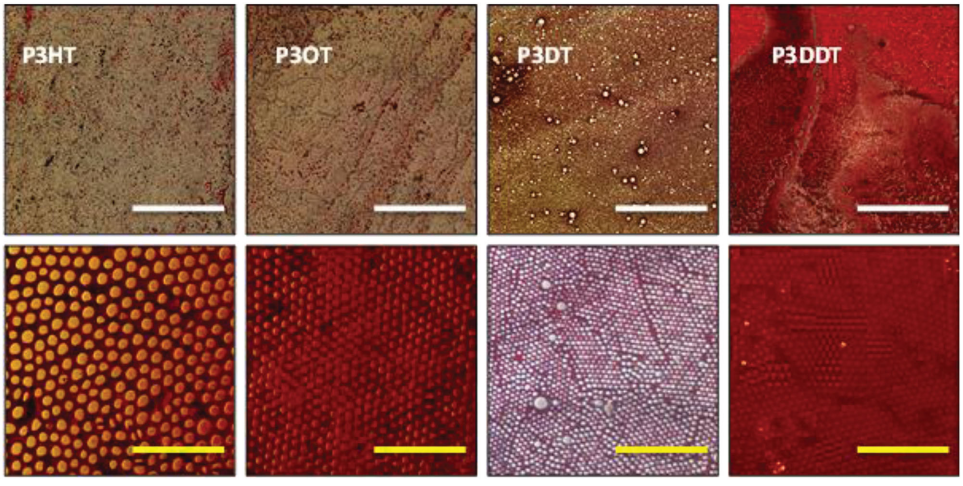

Figure 1. Optical (transmission) images of PT honeycomb thin films showing long-range ordered microporous structures. Top: low magnification; bottom: high magnification. Scale bars are 400 μm (top: white) and 40 μm (bottom: yellow).

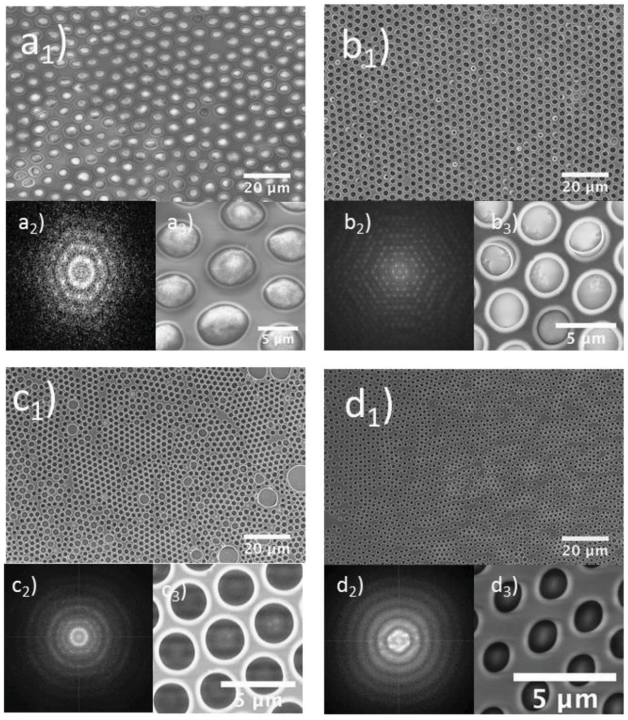

Figure 2. Scanning electron images of PT-based honeycomb films: a) P3HT, b) P3OT, c) P3DT, and d) P3DDT; subscript 2 for each image shows the FFT pattern calculated after converting the image. Subscript 3 shows zoomed-in image of single hexagonal lattice for each image.

order along with perfect 2D hexagonal ordering. A photograph of a P3OT honeycomb taken with an ordinary CCD camera shown in Figure S2 (Supporting Information), further demonstrates the long-range order of the BFT made thin films. In such films, areas as large as ≈5 × 5 mm^2 in size with highly regular honeycomb patterns are present, a size that is sufficient for future transitions of such films in sensory and photovoltaic devices. For the other PT derivatives, although they showed short-range order, the presence of diffused rings in their associated FFT pattern (Figure 2) indicated the presence of 2D disorder in the honeycomb film at large scale.

For P3OT we found favorable processing conditions to be in a wide range of humidity and airflow rate values when compared to P3HT which had a rather high tendency to coalesce. Processing conditions for P3DT and P3DDT were found to be more robust compared to P3HT but the order of honeycombs films and reproducibility from these polymers were not on par with P3OT. In order to make polymer solutions amenable for honeycomb formation, we needed to age them for at least seven days at room temperature, in dark. Except for P3HT, prolonged ageing of polymer solution leads to improved flexibility in processing conditions, including formation of thinner honeycomb films by the use of lower polymer concentration.[18b]

2.2. Pore Size Distribution and Order Parameter from Voronoi Tesselation

Pore sizes were found to vary with side chain length as observed in **Figure 3**. The longer the side chain, the smaller the pore size

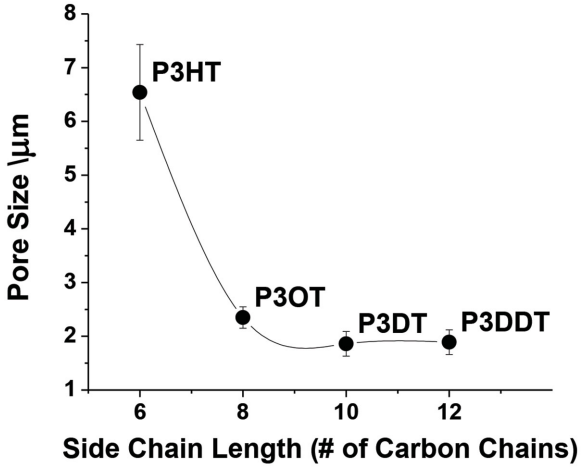

Figure 3. Pore size versus side chain length for PT-based honeycombs.

when these honeycombs were processed in similar conditions including concentration. Details on pore size estimation are given in the Supporting Information. It is worth noting that, there is a radial variation of pore size in such large size films due to changes in the evaporation rate from the edge to the center of the film, with the pore size increasing from edge to center (see Figure S3, Supporting Information).

One simple way to visualize the ordering of pores in 2D is by the use of Voronoi Tesselation (VT) method, a popular approach in computational geometry for modeling spatial structures, for pattern recognition, and for localization optimization.[20] In VT, a plane with n points is divided into convex polygons such as each polygon contains exactly one generating point and the vertices of each cell is equally spaced to its generating points. Given the input of the centroid of pores of the honeycomb, the VT method provides a graphical representation of nearest neighbors. The number of edges from each cell can be used to get the probability of having six nearest neighbors and the hexagonal packing can then be compared.[21] Also, with the probability of all possible nearest neighbors (NN), an order parameter (entropy, S) defined below can be used to assign each image in Figure 2

$$S = -\sum_{i=3}^{10} p_i \cdot \ln p_i \quad (1)$$

Here, p_i is the probability of finding i number of nearest neighbors. The smaller the order parameter S is, the more order the system exhibits. The observed variation of order parameter with side chain length (**Figure 4**b) and the probability of nearest neighbors (Figure 4a), both support the high hexagonal ordering seen in P3OT honeycomb films when compared to the rest of the PT-based honeycombs.

2.3. Crystalline versus Amorphous-Like Phase in PT-Based Honeycomb Films

Fluorescence emitted by a conjugated polymer is a property influenced by the extent of the π-conjugation system of the

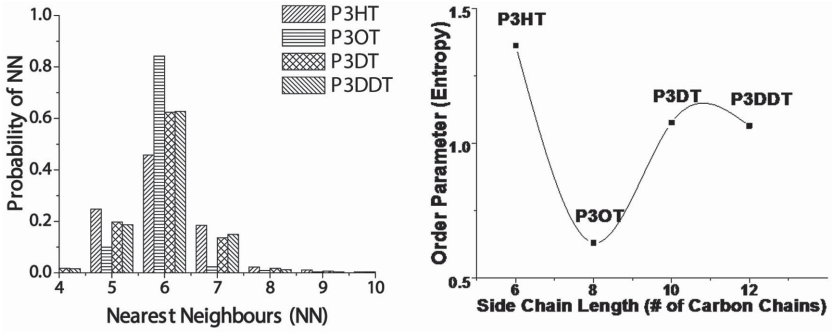

Figure 4. a) (left) Probability distribution of nearest neighbors in honeycomb films determined by Voronoi tessellation method. b) (right) Order parameter (entropy, *S*) calculated using nearest neighbor probability distribution. P3OT shows the lowest value of *S*, hence exhibits the most ordered film.

polymer backbone, and this can provide information on the polymer chain conformation or aggregation state or changes of such properties since such changes are usually accompanied by intra- or interchain quenching by energy transfer.[22] **Figure 5**a–d are images obtained by confocal fluorescence lifetime imaging microscopy (FLIM) for the honeycomb thin films process by BFT for the four PTs and Figure 5i–l are spatially resolved, confocal micro photoluminescence (PL) spectra measured at the honeycomb frame (black color) and hole (green color) from each of the PT-based honeycomb of these films. As a comparison, Figure S2 (Supporting Information) displays micro-PL spectra from the four PTs in solution and in drop-casted thin films. A detailed analysis of the micro-PL spectra and FLIM images in Figure 5 helps us to understand the heterogeneity in polymer aggregation state within (i) a given honeycomb and (ii) among various types of PT-based honeycombs which, as explained below, we can associate with (i) differences in polymer packing across

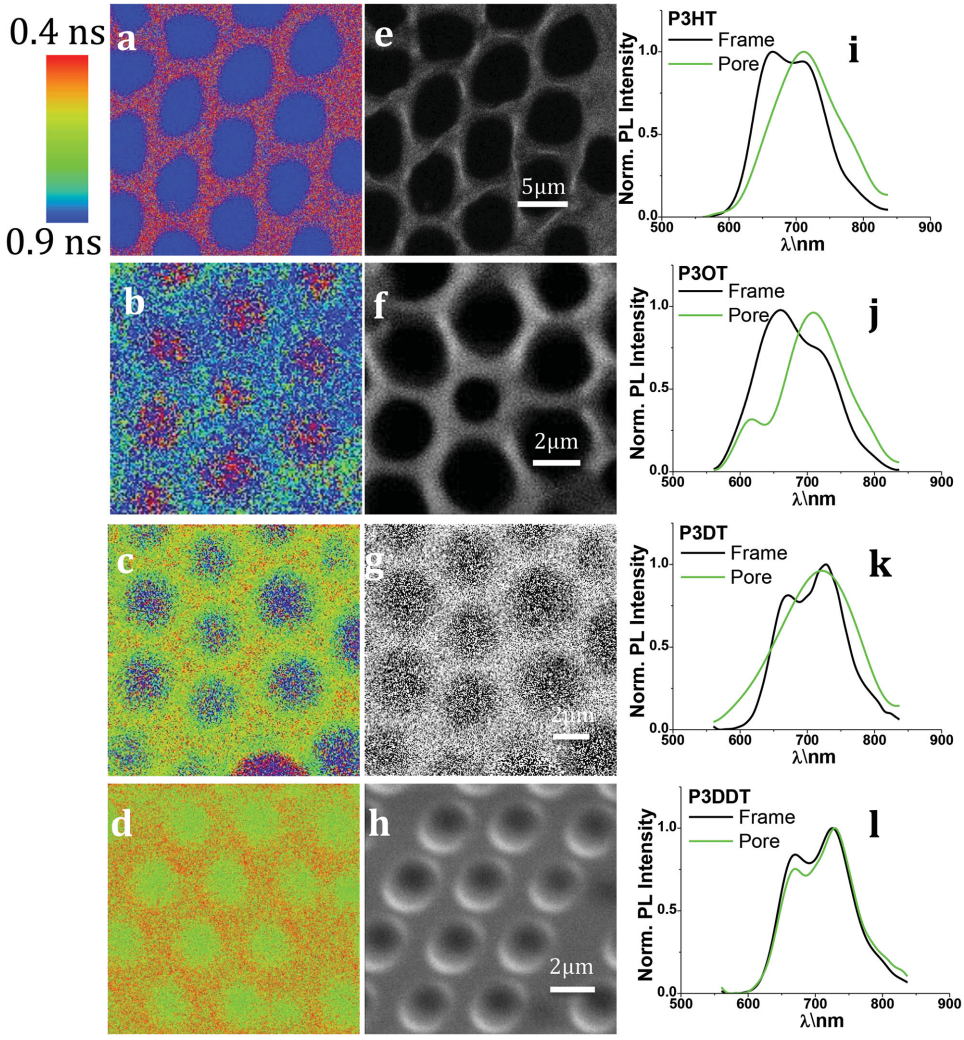

Figure 5. a–d) Confocal FLIM, e–h) confocal PL intensity image, and i–l) micro-PL spectroscopy of honeycomb thin films processed from: a,e,i) P3HT, b,f,j) P3OT, c,g,k) P3DT, and d,h,l) P3DDT. Micro-PL spectra were recorded at the frame (black color) and in the pore (green color) of the honeycomb cell units.

Table 1. PL parameters for solution, drop-cast, and honeycomb samples as derived from Figure 5 and Figure S3 (Supporting Information).

Sample	P3HT		P3OT		P3DT		P3DDT	
	τ_{PL}[a)] [ns]	R_{PL}[b)]	τ_{PL} [ns]	R_{PL}	τ_{PL} [ns]	R_{PL}	τ_{PL} [ns]	R_{PL}
Solution	0.58	–	0.58	–	0.58	–	0.58	–
Drop-cast	0.47	1.16	0.42	1.0	0.72	1.15	0.86	1.04
Honeycomb frame	0.75	1.06	0.42	1.3	0.81	0.8	0.64	0.84
Honeycomb hole	0.62	0.65	0.49	0.33	0.70	–	0.60	0.75

[a)] τ_{PL}, intensity averaged PL lifetime; [b)] R_{PL}, PL intensity ratio for high and low energy peaks in the PL spectrum.

the honeycomb framework and with (ii) differences in crystallinity among the four types of PTs and resulting from differences in side chain length. **Table 1** includes PL lifetimes (amplitude averaged values, see the Supporting Information for details) estimated from PL decays measured from diffraction-limited spots in the honeycomb frame and hole, and for a comparison from solution and drop-casted thin films for all four PTs. Freshly prepared polymer solutions exhibit PL lifetimes of about 0.66 ns which are rather long for PTs and which indicate CS_2 is a good solvent for all four PTs.[22b] Ageing (over seven days) decreases the PL lifetime to about 0.58 ns for all four PTs, most probably due to formation of self-quenched aggregates.[22b,23] PL spectra from either fresh or aged solutions are broad, with a single peak at around 590 nm (Figure S3, Supporting Information). Drop-casting any of the four PTs produces thin films with redshifted, bi-peak PL spectra with peaks @ 650 and 725 nm, previously assigned to vibronic, 0–0 and 0–1 transitions, respectively.[24] The ratio of these PL peaks in drop-casted films estimated from the micro-PL spectra from Figure S3 (Supporting Information) as R = PL@650nm/PL@725nm is in the range 1–1.1, e.g., $R \geq 1$ (see Table 1) which is common for 0–0 and 0–1 vibronic transitions associated with PL from aromatic molecules. PL lifetimes from drop-casted films increase in value with the increase in side chain length (Table 1, i.e., from P3HT to P3DDT) and an explanation for this phenomenon is given below. PT polymers including those studied here prefer to self-pack in solid phase in ordered, e.g., crystalline-like aggregates because of the strong π–π stacking of polymer backbones. π–π stacking promotes interchain quenching which in turn redshifts the PL spectrum in film compared to solution and decreases both the PL quantum yield and PL lifetime.[18b,25] An increase in polymer side chain length decreases π–π stacking interaction and this in turn decreases interchain quenching, leading to recovery (increase) of emitted PL, including the PL lifetime[26] (Table 1).

FLIM images from honeycomb PTs feature clear differences in PL lifetimes in the frame and in the holes (Figure 5a–d, insets, Table 1). Similarly, there are differences in the PL spectra measured in the frame and in the hole (Figure 5i–l, black vs green colored spectra). For P3HT, the PL spectrum measured in the frame is similar in shape to the drop-cast film PL spectrum (Figure 5i, black vs Figure S4, Supporting Information), with a ratio of the high and low energy peaks R = 1.1 and with these peaks spectrally shifted @ 660 and 710 nm, while the PL spectrum measured in the hole is broad, vibrationless, and single peaking @ 710 nm (Figure 5i). For P3OT, the PL spectrum measured in the frame is still bi-peak, with an $R > 1$, however, the PL spectrum from hole, while remaining bi-peak, now has an $R < 1$ (Figure 5j). For P3DT and P3DDT, the PL spectra in the frame are still bi-peak, but with an $R < 1$, while the PL spectra in the hole are single (@720 nm) and bi-peak, respectively (Figure 5k,l). The observation of single peak (@705–715 nm range) and bi-peak (@650 nm and @705–715 nm range) features in the PL spectra from PT honeycombs and of $R < 1$ values strongly suggests two polymer aggregation states are present in honeycomb films, amorphous-like disordered aggregate state and crystalline state,[27] whose contribution dictates the ratio R. This in turn reflects the presence of heterogeneity in crystallinity in PT honeycomb thin films. The polymer crystalline phase is similar to that usually observed in drop-casted films (Figure S4, Supporting Information), with a bi-peak spectrum with 0–0 and 0–1 vibronic transitions (@650 and 725 nm, respectively), while the amorphous-like phase has a broad, single peak at around 705–710 nm. Depending on the contribution of the two phases at a given place in the honeycomb film, the resulting spectrum might be bi-peak or single peak. For example, for P3HT, P3OT, and P3DT, the crystalline phase dominates in the frame, while the amorphous-like phase dominates in the hole. For P3DDT, the crystalline phase dominates both in frame and hole, since this framework shows rather large thickness in the hole regions (i.e., holes are not deep). We believe these differences in crystallinity arise from the different evaporation speeds of the solvent in the frame and in the holes which are imposed by BFT. Honeycomb frame is formed between adjacent water droplets which force a large amount of polymer material together to form a thick (≈1 μm) film following solvent and water evaporation. This provides evaporation rates similar to drop-casting, permitting the polymer to pack and form crystalline domains. In holes, solvent evaporation is faster because of less polymer material and as such the polymer has no time to crystallize, forming an amorphous phase. The idea of the presence of both crystalline and amorphous phase in PT honeycombs is also supported by the PL lifetimes observed in the frame and the hole, with PL lifetimes increasingly quenched in the latter case as one would expect from a self-quenched, redshifted aggregate.

P3OT is an exception, showing opposite behavior with respect to PL lifetimes of frame and holes and we may relate this with the high tendency of this particular polymer to form crystalline domains even in holes, at low concentration of polymer. Small and wide angle X-ray data (SAXS/WAXS)

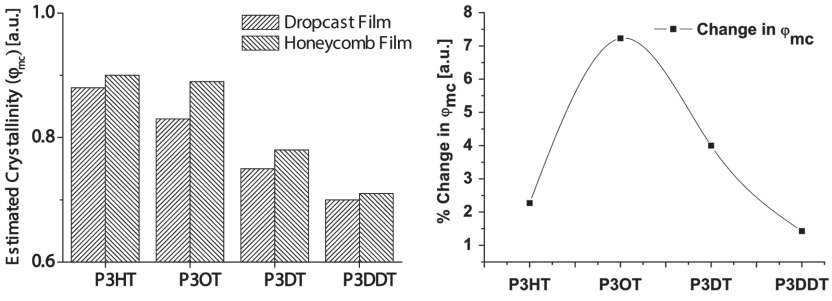

Figure 6. (Left) Crystallinity values (φ_{mc}) obtained from WAXS measurements of drop-cast and honeycomb PT-based thin films and (right) percent change in crystallinity value, φ_{mc}, from drop-cast to honeycomb PT-based thin films.

recorded from PT-based honeycomb and drop-cast films support our hypothesis, indicating increased crystallinity in honeycomb sample compared to drop-cast film, and this increase in crystallinity is more pronounced in the case of P3OT polymer (see **Figure 6** and Figure S5, Supporting Information, and details on crystallinity estimation by SAXS/WAXS).

3. Discussion

BFT has been demonstrated as a versatile, cost-effective method for producing ordered microporous structures with tunable pore size and frame thickness obtained through changes in processing parameters such as humidity, concentration of solution, temperature of substrate, or airflow rate.[11,15,18] The effect of these individual parameters has been evaluated extensively by many groups and on different types of polymers.[11d] Most of the BFT setups reported so far are very simple in nature and do not offer a precise reproduction of the morphology in the films due to inherent nonequilibrium nature of the evaporation process in the breath figure processing. BFT method is also susceptible to environmental factors when using non-PS based polymers, which provide less robust processing conditions to produce stabilized water droplets. Hence, in order to control the external environmental factors we designed a controlled humidity chamber where PT solutions were casted directly on substrates (Figure S1, Supporting Information). At constant humidity, the evaporation rate of the solution is affected by the airflow rate and by the surface temperature of the substrate. Controlling the flow rate is crucial and having a laminar flow helps obtain large-area honeycomb thin films. With the same experimental setup, we found possible to vary a whole range of parameters to explore the optimum parameters for achieving the best structures possible for a given polymer solution.

As shown by the SEM images in Figure 1, all four polymers are able to form honeycomb films by BFT after ageing, however, P3OT excels in hexagonal ordering and long-range (large area) thin film with hexagonally arranged porous structure as suggested by Voronoi Tesselation. P3OT also provides more robust processing conditions that allow modification of pore size by varying experimental parameters such as air flow, humidity, and concentration.

PTs prefer to form highly ordered aggregates in thin film phase due to their high tendency to $\pi-\pi$ stack their backbone. The result is polymer crystalline domains with improved charge mobility perpendicular to the stack.[27] Increasing the length of alkyl side chain in PTs decreases the $\pi-\pi$ stacking interaction and the crystallinity of the ordered phase, and this in turn might decrease charge mobility across the polymer stack but increases side chain ordering.[28] Side chain length modification changes the interaction between polymer chains, hence affecting polymer aggregation behavior.[29] Stenzel et al.[15a] suggested that for amphiphilic polymers aggregation is a key condition in suppressing coalescence and leading to the formation of stable honeycomb films. PTs are also known to develop aggregation in mixed solvents where using such approach PT whiskers could be formed by ageing up to two months in anisole solution.[30] In the present study, we found that PTs have such aggregation behavior in solution even with the use of a good solvent, if the solution is left to age for 7–10 days. Therefore, we believe that for hydrophobic polymers like alkyl-substituted PTs, breath figure technique becomes successful if the polymer is dissolved in a good solvent and aged for a considerable period of time (days or even weeks). Such aggregates stop the coalescence and allow formation of stable ordered microdroplets. We found that by removing these aggregates by filtration, for example, by the use of a 0.45 µm porous filter, the resulting solution was incapable of forming stable microporous structures.

During the processing of dynamic breath figure technique, the surface temperature is in the range of –6 to 0 °C.[8] This low temperature arises due to evaporative cooling and makes the condensation of water droplets feasible at the solution–air interface. In this study, condensation is augmented by using a cold stage along with evaporative cooling. In the above defined temperature range, the polymer with the glass transition temperature (T_g) lower but closest to the temperature of the substrate should easily form breath figures. Changing the side chain also changes polymer's T_g.[31] For PTs used in the present study, **Table 2** lists T_g values found in literature,[32] according to which we now understand why P3DDT did not form large-area honeycombs, given its very low T_g of –19 °C, a temperature unachievable during the evaporative cooling. Thus, among the polythiophenes considered in the present study, P3OT appears to have the right combination of side chain length and T_g, the former helping in promoting aggregates in the aged solution of "perfect" size, the latter being closest to the surface temperature where condensation happens. The result is large area (over 5×5 mm^2) perfectly organized P3OT honeycombs. Both of

Table 2. Glass transition temperatures of polythiophene derivatives.[32]

Polymer	T_g
P3HT	20.3 °C
P3OT	–9.2 °C
P3DT	–
P3DDT	–19 °C

these properties compete together and hence P3OT seems to have optimum side chain length to form most perfect breath figures out of the investigated PTs. The effect of side chain of polythiophenes on film morphology and optical properties has been studied widely in the bulk form[33] as well as at the single polymer chain levels.[19a,34] Here, through optical and structural studies, we found clear differences in the polymer aggregation phase in the honeycomb framework, highly crystalline in the frame and a combination of amorphous and crystalline in the hole, with the ratio of amorphous to crystalline phases changing with the polymer side chain length.

4. Conclusion

Herein, we provided a clear demonstration of how a relatively inexpensive process such as BFT can be realized as a repeatable method to produce microporous films from hydrophobic conjugated polymers, presenting for the first time semitransparent honeycombs with area dimensions suitable for photovoltaic and sensory devices, with almost perfect organization of pores over sub-cm sized domains, which achievable by other methods like microlithography would be rather costly. Here, we studied the effect of side chain length of PT on the breath figure forming capability. For PTs, a six-carbon long side chain like P3HT is known to provide optimal performance for photovoltaic applications, but we found in the present study that it is not best suited for honeycomb formation. Most probably, such short chain confers the polymer a high glass transition temperature which is unfavorable for aggregate formation. P3OT, the PT with a side chain length of eight carbon chains (P3OT) is better for honeycomb formation. Using a combination of optical and structural characterization methods, we demonstrated different polymer aggregation phases in the honeycomb framework, whose contributions change with the polymer side chain length.

One can envision semitransparent photovoltaic devices made out of breath figure polythiophene films doped with fullerenes or other semiconducting n-type nanomaterials or sensory devices based on such microporous films doped with energy transfer relevant nanoparticles. Since BFT-based microporous film offers a larger (≈140%) surface area compared to a planar (drop-cast/spin-cast film) due to its unique 3D structure, this in turn is expected to increase the efficiency of semitransparent photovoltaic devices or sensitivity in sensory devices incorporating such breath figure films.

5. Experimental Section

Materials and Honeycomb Film Preparation by BFT: Commercially available polythiophenes were bought from Rieke Metals and carbon disulfide (CS_2) was from Sigma-Aldrich. All polymers have an average molecular weight of 70 000–90 000 with regioregularity of ≈96%. Each of the four polymers was dissolved in CS_2 with the help of magnetic stirring and stored in an airtight vial for ageing. Aged solutions (7 d on average) were drop-casted using breath figure technique on glass or metal oxide surfaces and exposed to controlled humidity, temperature, and airflow in order to preserve the order of honeycomb films. The films were made in ambient air and immediately kept into vacuum tight boxes after the deposition was complete. Drop-cast samples of polymer solutions on glass substrates were exposed to laminar air flow with controlled humidity. In order to control the physical parameters of the experiment, a home-built setup was used which is pictured in Figure S1 (Supporting Information). A glove box was connected to a humidifier and dehumidifier, which were controlled by a microcontroller to produce ±1% relative humidity variation. A laminar flow control box was designed to control the airflow rate. Furthermore, the substrate holder was temperature controlled using water-cooled copper plate. To compare the effect of side chain on honeycomb formation capability, all polythiophene polymers were cast using the following processing parameters: Concentration: 2 mg mL^{-1}; relative humidity: 65%; air flow rate: 2 L min^{-1}; substrate holder (copper) temperature: 14 °C; substrate: 9 nm MoO_3 thin layer coated on glass cover slips of 0.17 mm thickness; and volume of solution cast on substrate: 25 µL.

Methods: Confocal FLIM and micro-PL spectroscopy studies were carried out using a custom-built scanning-stage inverted microscope described elsewhere.[18b] Samples were illuminated with 440 nm pulsed light from a solid-state diode laser (LDH-440 Picoquant) using a 0.9 NA 60× dry objective lens (Olympus America). Fluorescence from the samples was collected by the same lens, filtered from laser excitation by a dichroic (532DRLP, Semrock) and by a band-pass filter (FF01-532RLP, Semrock), spatially filtered by a 5 µm pinhole, and finally refocused onto a single-photon-counting avalanche photodiode (MPD, Picoquant). FLIM was carried on samples under nitrogen atmosphere to avoid photodegradation. FLIM images were acquired and analyzed with the commercial Symphotime 5.32 software (Picoquant). PL lifetimes reported in here were calculated as amplitude average lifetimes following double exponential fits. Micro-PL spectra were acquired by a Spectra Pro 2300i spectrograph coupled to a back-illuminated CCD camera (Roper Scientific, PIXIS 100) by directing the collected fluorescence via a side port of the microscope and through a 5 µm pinhole. SEM was performed with a Hitachi S-4800 SEM and with a 3 nm Ag coating layer deposited on top of PT-based honeycomb films for improved conductivity. SAXS/WAXS measurements were carried out on a Bruker-AXS Nanostar U instrument equipped with a Cu rotating anode, a Vantech 2000 detector, and operated in the high-resolution configuration and short detector distance. The camera length for the instrument was calibrated using silver behenate. Polymer thin films were delaminated from the MoO_3 coated glass substrates using KOH treatment and careful rinsing in DI water, SAXS/WAXS signals were recorded from free-standing films in transmission mode. Details on data analysis are given in the Supporting Information.

Supporting Information

Supporting Information is available from the Wiley Online Library or from the author.

Acknowledgements

Research carried out at the Center for Functional Nanomaterials, Brookhaven National Laboratory and supported by the U.S. Department of Energy by Contract No. DE-SC0012704. Funding provided in part through a BNL/SBU seed grant and SMART Grid project (P.K.R. and T.A.V.).

Received: June 16, 2015
Revised: July 22, 2015
Published online: September 1, 2015

[1] a) A. Bolognesi, C. Mercogliano, S. Yunus, M. Civardi, D. Comoretto, A. Turturro, *Langmuir* **2005**, *21*, 3480; b) L. A. Connal, G. G. Qiao, *Adv. Mater.* **2006**, *18*, 3024.

[2] V. P. Shastri, I. Martin, R. Langer, *Proc. Natl. Acad. Sci. USA* **2000**, *97*, 1970.
[3] L.-S. Wan, Q.-L. Li, P.-C. Chen, Z.-K. Xu, *Chem. Commun.* **2012**, *48*, 4417.
[4] a) H. Yabu, M. Takebayashi, M. Tanaka, M. Shimomura, *Langmuir* **2005**, *21*, 3235; b) H. Yabu, M. Shimomura, *Chem. Mater.* **2005**, *17*, 5231; c) M. Ma, R. M. Hill, *Curr. Opin. Colloid Interface Sci.* **2006**, *11*, 193.
[5] a) M. Yoshida, M. Asano, A. Safranj, H. Omichi, R. Spohr, J. Vetter, R. Katakai, *Macromolecules* **1996**, *29*, 8987; b) H. Bai, C. Du, A. Zhang, L. Li, *Angew. Chem.* **2013**, *52*, 12240.
[6] a) T. Ohzono, T. Nishikawa, M. Shimomura, *J. Mater. Sci.* **2004**, *39*, 2243; b) M. Campbell, D. N. Sharp, M. T. Harrison, R. G. Denning, A. J. Turberfield, *Nature* **2000**, *404*, 53; c) T. Cao, F. Wei, X. Jiao, J. Chen, W. Liao, X. Zhao, W. Cao, *Langmuir* **2003**, *19*, 8127; d) Z. Nie, E. Kumacheva, *Nat. Mater.* **2008**, *7*, 277.
[7] M. L. Hoa, M. Lu, Y. Zhang, *Adv. Colloid Interface Sci.* **2006**, *121*, 9.
[8] U. H. F. Bunz, *Adv. Mater.* **2006**, *18*, 973.
[9] a) D. Fritter, C. M. Knobler, D. A. Beysens, *Phys. Rev. A* **1991**, *43*, 2858; b) A. Steyer, P. Guenoun, D. Beysens, C. M. Knobler, *Phys. Rev. B* **1990**, *42*, 1086.
[10] M. Hernandez-Guerrero, M. H. Stenzel, *Polym. Chem.* **2012**, *3*, 563.
[11] a) M. H. Stenzel, C. Barner-Kowollik, T. P. Davis, *J. Polym. Sci., Part A: Polym. Chem.* **2006**, *44*, 2363; b) L. S. Wan, L. W. Zhu, Y. Ou, Z. K. Xu, *Chem. Commun.* **2014**, *50*, 4024; c) P. Escalé, L. Rubatat, L. Billon, M. Save, *Eur. Polym. J.* **2012**, *48*, 1001; d) A. Muñoz-Bonilla, M. Fernández-García, J. Rodríguez-Hernández, *Prog. Polym. Sci.* **2014**, *39*, 510.
[12] H. Battenbo, R. J. Cobley, S. P. Wilks, *Soft Matter* **2011**, *7*, 10864.
[13] G. Widawski, M. Rawiso, B. Francois, *Nature* **1994**, *369*, 387.
[14] J. Peng, Y. C. Han, Y. M. Yang, B. Y. Li, *Polymer* **2004**, *45*, 447.
[15] a) M. H. Stenzel, *Aust. J. Chem.* **2002**, *55*, 239; b) X. Y. Zhao, Q. Cai, G. X. Shi, Y. Q. Shi, G. W. Chen, *J. Appl. Polym. Sci.* **2003**, *90*, 1846; c) T. Nishikawa, J. Nishida, R. Ookura, S.-I. Nishimura, V. Scheumann, M. Zizlsperger, R. Lawall, W. Knoll, M. Shimomura, *Langmuir* **2000**, *16*, 1337; d) O. Karthaus, X. Cieren, N. Maruyama, M. Shimomura, *Mater. Sci. Eng., C* **1999**, *10*, 103; e) A. Böker, Y. Lin, K. Chiapperini, R. Horowitz, M. Thompson, V. Carreon, T. Xu, C. Abetz, H. Skaff, A. D. Dinsmore, T. Emrick, T. P. Russell, *Nat. Mater.* **2004**, *3*, 302.
[16] a) J. Y. Ding, A. J. Zhang, H. Bai, L. Li, J. Li, Z. Ma, *Soft Matter* **2013**, *9*, 506; b) A. Zhang, C. Du, H. Bai, Y. Wang, J. Wang, L. Li, *ACS Appl. Mater. Interfaces* **2014**, *6*, 8921.
[17] a) J. Ding, J. Gong, H. Bai, L. Li, Y. Zhong, Z. Ma, V. Svrcek, *J. Colloid Interface Sci.* **2012**, *380*, 99; b) L. A. Connal, R. Vestberg, C. J. Hawker, G. G. Qiao, *Macromolecules* **2007**, *40*, 7855.
[18] a) M. H. Nurmawati, R. Renu, P. K. Ajikumar, S. Sindhu, F. C. Cheong, C. H. Sow, S. Valiyaveettil, *Adv. Funct. Mater.* **2006**, *16*, 2340; b) H. Tsai, Z. Xu, R. K. Pai, L. Wang, A. M. Dattelbaum, A. P. Shreve, H.-L. Wang, M. Cotlet, *Chem. Mater.* **2011**, *23*, 759; c) L. Song, R. K. Bly, J. N. Wilson, S. Bakbak, J. O. Park, M. Srinivasarao, U. H. F. Bunz, *Adv. Mater.* **2004**, *16*, 115; d) Y. Lu, L. Wang, B. Zhao, G. Xiao, Y. Ren, X. Wang, C. Li, *Thin Solid Films* **2008**, *516*, 6365; e) B. Erdogan, L. Song, J. N. Wilson, J. O. Park, M. Srinivasarao, U. H. F. Bunz, *J. Am. Chem. Soc.* **2004**, *126*, 3678.
[19] a) T. Adachi, J. Brazard, R. J. Ono, B. Hanson, M. C. Traub, Z.-Q. Wu, Z. Li, J. C. Bolinger, V. Ganesan, C. W. Bielawski, D. A. Vanden Bout, P. F. Barbara, *J. Phys. Chem. Lett.* **2011**, *2*, 1400; b) I. F. Perepichka, D. F. Perepichka, H. Meng, F. Wudl, *Adv. Mater.* **2005**, *17*, 2281; c) M. Jaymand, M. Hatamzadeh, Y. Omidi, *Prog. Polym. Sci.* **2015**, 47, 26.
[20] A. Okabe, B. Boots, K. Sugihara, S. N. Chiu, *Spatial Tesselations: Concepts and Applications of Voronoi Diagrams*, 2nd ed., Wiley, Chichester, UK **2000**.
[21] A. J. Krejci, C. G. W. Thomas, J. H. Dickerson, *Phys. Rev. E* **2013**, *87*, 042307.
[22] a) H. Jiang, P. Taranekar, J. R. Reynolds, K. S. Schanze, *Angew. Chem., Int. Ed.* **2009**, *48*, 4300; b) Z. Xu, H. Tsai, H.-L. Wang, M. Cotlet, *J. Phys. Chem. B* **2010**, *114*, 11746.
[23] a) P.-T. Huang, Y.-S. Chang, C.-W. Chou, *J. Appl. Polym. Sci.* **2011**, *122*, 233; b) F. Wang, G. C. Bazan, *J. Am. Chem. Soc.* **2006**, *128*, 15786.
[24] a) J. Clark, C. Silva, R. H. Friend, F. C. Spano, *Phys. Rev. Lett.* **2007**, *98*, 206406; b) C. Carach, M. J. Gordon, *J. Phys. Chem. B* **2013**, *117*, 1950.
[25] a) X. M. Jiang, R. Österbacka, C. P. An, Z. V. Vardeny, *Synth. Met.* **2003**, *137*, 1465; b) G. Rumbles, I. D. W. Samuel, L. Magnani, K. A. Murray, A. J. DeMello, B. Crystall, S. C. Moratti, B. M. Stone, A. B. Holmes, R. H. Friend, *Synth. Met.* **1996**, *76*, 47.
[26] Y.-Z. Ma, R. W. Shaw, X. Yu, H. M. O'Neill, K. Hong, *J. Phys. Chem. B* **2012**, *116*, 14451.
[27] R. Noriega, J. Rivnay, K. Vandewal, F. P. V. Koch, N. Stingelin, P. Smith, M. F. Toney, A. Salleo, *Nat. Mater.* **2013**, *12*, 1038.
[28] a) Y. D. Park, D. H. Kim, Y. Jang, J. H. Cho, M. Hwang, H. S. Lee, J. A. Lim, K. Cho, *Org. Electron.* **2006**, *7*, 514; b) R. J. Kline, M. D. McGehee, E. N. Kadnikova, J. Liu, J. M. J. Fréchet, *Adv. Mater.* **2003**, *15*, 1519.
[29] T. Yamamoto, D. Komarudin, M. Arai, B.-L. Lee, H. Suganuma, N. Asakawa, Y. Inoue, K. Kubota, S. Sasaki, T. Fukuda, H. Matsuda, *J. Am. Chem. Soc.* **1998**, *120*, 2047.
[30] M. He, J. Ge, M. Fang, F. Qiu, Y. Yang, *Polymer* **2010**, *51*, 2236.
[31] S. Malik, A. K. Nandi, *J. Polym. Sci., Part B: Polym. Phys.* **2002**, *40*, 2073.
[32] a) R. Payerne, M. Brun, P. Rannou, R. Baptist, B. Grévin, *Synth. Met.* **2004**, *146*, 311; b) S. Pal, S. Roy, A. K. Nandi, *J. Phys. Chem. B* **2005**, *109*, 18332.
[33] a) H.-J. Wang, L.-H. Chan, C.-P. Chen, S.-L. Lin, R.-H. Lee, R.-J. Jeng, *Polymer* **2011**, *52*, 326; b) W. Y. Huang, C. C. Lee, S. G. Wang, Y. K. Han, M. Y. Chang, *J. Electrochem. Soc.* **2010**, *157*, B1336.
[34] M. Vacha, S. Habuchi, *NPG Asia Mater.* **2010**, *2*, 134.